

We are IntechOpen, the world's leading publisher of Open Access books Built by scientists, for scientists

6,900

Open access books available

186,000

International authors and editors

200M

Downloads

Our authors are among the

154

Countries delivered to

TOP 1%

most cited scientists

12.2%

Contributors from top 500 universities



WEB OF SCIENCE™

Selection of our books indexed in the Book Citation Index
in Web of Science™ Core Collection (BKCI)

Interested in publishing with us?
Contact book.department@intechopen.com

Numbers displayed above are based on latest data collected.
For more information visit www.intechopen.com



Doped Semiconductor Nanocrystals: Development and Applications

*Anielle C.A. Silva, Eliete A. Alvin,
Francisco R.A. dos Santos, Samanta L.M. de Matos,
Jerusa M. de Oliveira, Alessandra S. Silva, Éder V. Guimarães,
Mirella S. Vieira, Eurípedes A. da Silva Filho,
Ricardo S. Silva, Lucas Anhezini, Nilvanira D. Tebaldi
and Noelio O. Dantas*

Abstract

This chapter aims to show significant progress that our group has been developing and the applications of several doped semiconductor nanocrystals (NCs), as nanopowders or embedded in glass systems. Depending on the type of dopant incorporated in the nanocrystals, the physical, chemical, and biological properties can be intensified. However, it can also generate undesired toxic effects that can potentially compromise its use. Here we present the potential of zinc oxide NCs doped with silver (Ag), gold (Au), and magnesium (Mg) ions to control bacterial diseases in agriculture. We have also performed biocompatibility analysis of the pure and Ag-doped sodium titanate ($\text{Na}_2\text{Ti}_3\text{O}_7$) NCs in *Drosophila*. The doped nanocrystals embedded in glassy systems are chrome (Cr) or copper (Cu) in ZnTe and Bi_2Te_3 NCs for spintronic development nanodevices. Therefore, we will show several advantages that doped nanocrystals may present in the technological and biotechnological areas.

Keywords: doping, semiconductor nanocrystals, agriculture, biological effects, development, glass system, nanopowders

1. Introduction

The development of new nanocrystals made from the doping of ions in semiconductors creates interesting physical–chemical properties and biological effects. The nanopowders are aiming at agricultural applications, and doped nanocrystals embedded in the glass system can be used in spintronics applications.

Bacterial diseases of plants occur in every place that is reasonably moist or warm, and they affect all kinds of plants. Bacterial diseases are prevalent and severe in the humid tropics, but they may be extremely destructive anywhere under favorable environmental conditions [1]. Control bacterial diseases in agriculture are complex because the few registered chemical products and the nanoparticles or nanocrystals emerge as an innovative method in disease management. Zinc-oxide (ZnO) nanoparticles or nanocrystals are among the most commonly used [2–5].

ZnO, ZnS, or MgO nanoparticles have previously been used to control plant diseases caused by *Liberibacter crescens* [6], *Xanthomonas alfalfae subsp. citrumelonis* and *Pseudomonas syringae* [7], *Xanthomonas perforans* [8], *Xanthomonas campestris pv. Campestris* [9], *Pantoea ananatis* [10, 11], *Xanthomonas axonopodis pv. Citri* [12], *Xanthomonas oryzae pv. Oryzae* [13], and *Xanthomonas citri subsp. Citri* [14]. ZnO nanocrystals (NCs) may be doped with various elements, such as noble metals or transition metals, to increase their bactericidal effect. Doping is a process that consists of adding new elements to the nanoparticle's structure and changing their chemical characteristics [2]. Therefore, in this chapter book, we will show the results of ZnO NCs doped with silver (Ag), gold (Au), and magnesium (Mg) ions to control bacterial diseases in agriculture.

The fruit fly *Drosophila melanogaster* is a well-established model organism in various areas of science, including nanotoxicology [15]. The fruit fly also has 77% of the conserved genes related to human diseases [16] and considerable similarities with humans in different physiological mechanisms [17].

Several mutant lines for a broad range of human diseases are available in this model, besides its low cost and easy maintenance in the laboratory, in addition to a short life cycle, when compared to other model organisms such as fishes and mammals. Taken together, these characteristics make *Drosophila* a valuable model for studies that evaluate long-term and developmental effects in nanotoxicology [15]. Here we present results regarding the biocompatibility analysis of the pure and Ag-doped $\text{Na}_2\text{Ti}_3\text{O}_7$ nanocrystals in *Drosophila*.

The doped nanocrystals can be embedded in glassy systems, allowing for various applicability in devices. $\text{Zn}_{1-x}\text{A}_x\text{Te}$ ($\text{A} = \text{Cr}; \text{Cu}$) nanocrystals (NCs) have been one investigated diluted magnetic semiconductor (DMS) system, due mainly to their strengthening *sp-d* exchange interactions with increasing A-doping concentration [18]. Cr and Cu-doped NCs simultaneously exhibit semiconductor and magnetic properties that may allow more diverse technological applications than undoped semiconductors [19, 20]. In this context, we present a very effective method for the growth of Cr^{2+} and Cu^{2+} ions-doped ZnTe NCs in a glass system ($65\text{P}_2\text{O}_5 \cdot 14\text{ZnO} \cdot 1\text{Al}_2\text{O}_3 \cdot 10\text{BaO} \cdot 10\text{PbO}$ (mol %), named PZABP) using the fusion nucleation method, as descriptions in Refs. [21, 22].

Bi_2Te_3 semiconductors at the nanoscale are highly performing materials for thermoelectric and promising applications as topological insulators [23]. These nano-semiconductors' physical and chemical properties can enhance and perform new features based on quantum behavior and the electronic structure's doping [24–26]. The synthesis of Bi_2Te_3 NCs in diamagnetic host glasses allows the samples' high chemical stability. During fusion, Cr ions can incorporate into these systems allowing possible applications in the manufacture of magneto-optical devices [25–27]. Therefore, the long-range magnetic properties generated by the domain of the Cr ion doping spins, in addition to the insulating topological states of the Bi_2Te_3 semiconductor NCs, have aroused great interest in the scientific community for the development of spintronic nanodevices [24, 27, 28]. Thus, we will show some results of Cr doped Bi_2Te_3 NCs.

Therefore, in this chapter, we show doped nanocrystals' results in powdered or embedded glass systems aiming at several applications.

2. Nanocrystals in powder or embedded in glass systems

Depending on how these nanocrystals are, for example, powdered or embedded in glass systems, the applicability is diverse. Thus, in applications in agronomy, dental, or biology, these doped nanocrystals must be in powder to be dispersed or not in solutions. In applications such as spintronics, the doped nanocrystals must be embedded in

a thermally and chemically stable system, such as a glass system. We will comment on these peculiarities and advantages of each doped nanocrystal in the following sections.

2.1 Synthesis of Nanopowders and nanocrystals embedded in glassy matrices

2.1.1 Synthesis of Nanopowders

The pure and doped ZnO NCs were synthesized by coprecipitation by reference [29]. Pure and doped sodium titanate ($\text{Na}_2\text{Ti}_3\text{O}_7$) were synthesized by reference [30].

2.1.2 Synthesis of Cr or Cu-doped ZnTe nanocrystals embedded in glass matrix

The PZABP glass matrix with a nominal composition of $65\text{P}_2\text{O}_5 \cdot 14\text{ZnO} \cdot 1\text{Al}_2\text{O}_3 \cdot 10\text{BaO} \cdot 10\text{PbO}$ (mol %) adding 2Te (wt %), and Cr or Cu at doping x content varying with Zn content from 0 to 10 (wt %), were synthesized by fusion in alumina crucibles at 1300 °C for 30 minutes. These melted mixtures were quickly cooled to room temperature forming a glass system doped with the precursor ions needed for nanoparticle growth. Next, the glass samples were thermally annealed at 500 °C for 10 hours to enhance the diffusion of Zn^{2+} , Cr^{2+} or Cu^{2+} and Te^{2-} ions throughout the host PZABP matrix and induce the growth of $\text{Zn}_{1-x}\text{Cr}_x\text{Te}/\text{Zn}_{1-x}\text{Cu}_x\text{Te}$ NCs. The physical properties of the glass samples were studied by optical absorption (OA), recorded with a model UV-3600 Shimadzu UV-VIS-NIR spectrometer, operating between 190 and 3300 nm; XRD patterns were recorded using a XRD-6000 Shimadzu diffractometer equipped with monochromatic $\text{CuK}_{\alpha 1}$ radiation ($k = 1.54056 \text{ \AA}$) and set to a resolution of 0.02; Transmission electron micrographs (TEM JOEL, JEM-2100, 200 kV) and EPR measurements at temperature of 10 K were performed with a high sensitivity Bruker-EMX spectrometer operating at X-band (9.4 GHz) microwave frequency.

2.1.3 Synthesis of Cr-doped Bi_2Te_3 nanocrystals embedded in glass matrix

$\text{Bi}_{2-x}\text{Cr}_x\text{Te}_3$ NCs were synthesized by the fusion method in a borosilicate glass matrix with the following nominal composition: $\text{SNAB-}45\text{SiO}_2 \cdot 30\text{Na}_2\text{CO}_3 \cdot 5\text{Al}_2\text{O}_3 \cdot 20\text{B}_2\text{O}_3$ (mol %), 2% (of the weight of the glass matrix) of Te and Bi_2O_3 , with nominal Cr content of x ($x = 0.00, 0.01, \text{ and } 0.05$) as a function of bismuth concentration. The powdered glass and NC precursors were mixed together and melted in an alumina crucible at 1200 °C for 30 min and then rapidly cooled to room temperature, permitting the formation of Cr-doped Bi_2Te_3 NCs.

2.1.4 Synthesis of Cr-doped Bi_2Te_3 nanocrystals embedded in glass matrix

$\text{Bi}_{2-x}\text{Cr}_x\text{Te}_3$ NCs were synthesized by the fusion method in a borosilicate glass matrix with the following nominal composition: $\text{SNAB-}45\text{SiO}_2 \cdot 30\text{Na}_2\text{CO}_3 \cdot 5\text{Al}_2\text{O}_3 \cdot 20\text{B}_2\text{O}_3$ (mol %), 2% (of the weight of the glass matrix) of Te and Bi_2O_3 , with nominal Cr content of x ($x = 0.00, 0.01, \text{ and } 0.05$) as a function of bismuth concentration. The powdered glass and NC precursors were mixed together and melted in an alumina crucible at 1200 °C for 30 min and then rapidly cooled to room temperature, permitting the formation of Cr-doped Bi_2Te_3 NCs.

2.1.5 Nanocrystals for the control plant bacterial disease

To evaluate the growth inhibition zone of *Xanthomonas campestris pv. campestris* *in vitro*, a basic layer of 2% agar-water medium and semi-solid nutrient medium (0.8%)

with 10% of the bacterial suspension (10^8 CFU/mL) was added to Petri dishes. Seven disks of sterile filter paper (6 mm) were embedded with 10 μ L of solution Ag-doped ZnO NCs, and Au-doped ZnO NCs, at 100; 10; 1; 0.1; and 0.01 mg/mL, and incubated at 28 °C for 48 hours. The diameter of the inhibition zone was measured.

In the greenhouse, tomato plants (three- to four-leaf stage) were sprayed with Mg-doped ZnO NCs at 2.5 mg/mL, and three days later, the plants were inoculated with a *Xanthomonas gardneri*-bacterial suspension (10^9 CFU/mL). The severity of the disease was analyzed.

2.1.6 *In vivo* biocompatibility analysis in *Drosophila melanogaster*

We have performed a developmental assay to evaluate whether Na_2TiO_7 and $\text{Na}_2\text{TiO}_7\text{:Ag}$ could present any toxicity *in vivo*. Adult males and females were conditioned and kept in oviposition plates for six hours. After 24 hours of controlled oviposition, first instar larvae (L1) were carefully transferred (six replicates per concentration containing 30 larvae each) to standard *Drosophila* medium containing Na_2TiO_7 and $\text{Na}_2\text{TiO}_7\text{:Ag}$ at the final concentration of 0.02 mg/mL (66.30 μ mol/L) while control larvae were transferred to a standard culture medium. The animals developed through all larval stages during the following 4 days, while they actively fed until reaching the pupal stage. Animals that reached pupal stage were counted daily and it was possible to determine total pupation and daily pupation rate. We obtained the larval lethality rate by subtracting the number of pupae from the initial larvae number. After pupal metamorphosis, the animals emerge as adults and were transferred to a standard media and monitored throughout its adult lives to perform the adult lifespan assay. Deaths were counted daily until all animals were dead.

2.2 Nanocrystals in powder: Development and applicability

In this section, we will show the results of ZnO NCs doped with silver (Ag), gold (Au), and magnesium (Mg) ions to control bacterial diseases in agriculture. We will also present *in vivo* biocompatibility assays of pure and Ag-doped $\text{Na}_2\text{Ti}_3\text{O}_7$ nanocrystals in *Drosophila* development.

2.2.1 Nanocrystals application in agriculture to control bacterial diseases

The nanocrystals of ZnO in this work have a wurtzite structure, and silver (Ag), gold (Au), and magnesium (Mg) ions were doped in ZnO NCs, as shown in **Figure 1a**. The Ag or Au doped ZnO NCs inhibited *Xanthomonas campestris pv. campestris* growth, at 100 and 10 mg/mL (**Figure 1b,c**). Other elements can also inhibit, such as, Mg ions that inhibited the growth of *Xanthomonas gardneri*, and reduced the severity of tomato bacterial spot (**Figure 1e**), and controlled the bacteria present in tomato seeds [31]. Therefore, nanotechnology could sustainably mitigate many challenges in disease management by reducing agrochemical use [32].

2.2.2 Biocompatibility *In Vivo* of nanocrystals

The crystalline structure of pure and silver (Ag) doped sodium titanate ($\text{Na}_2\text{Ti}_3\text{O}_7$) is shown in **Figure 2a**. The Ag ions replace sodium (Na) or titanium (Ti) ions in sodium titanate's crystalline structure.

In order to investigate whether $\text{Na}_2\text{Ti}_3\text{O}_7$ and Ag-doped $\text{Na}_2\text{Ti}_3\text{O}_7$ nanocrystals could be biocompatible, we performed a bioassay to evaluate the effects of these NCs during *Drosophila* development. Surprisingly, the animals that developed

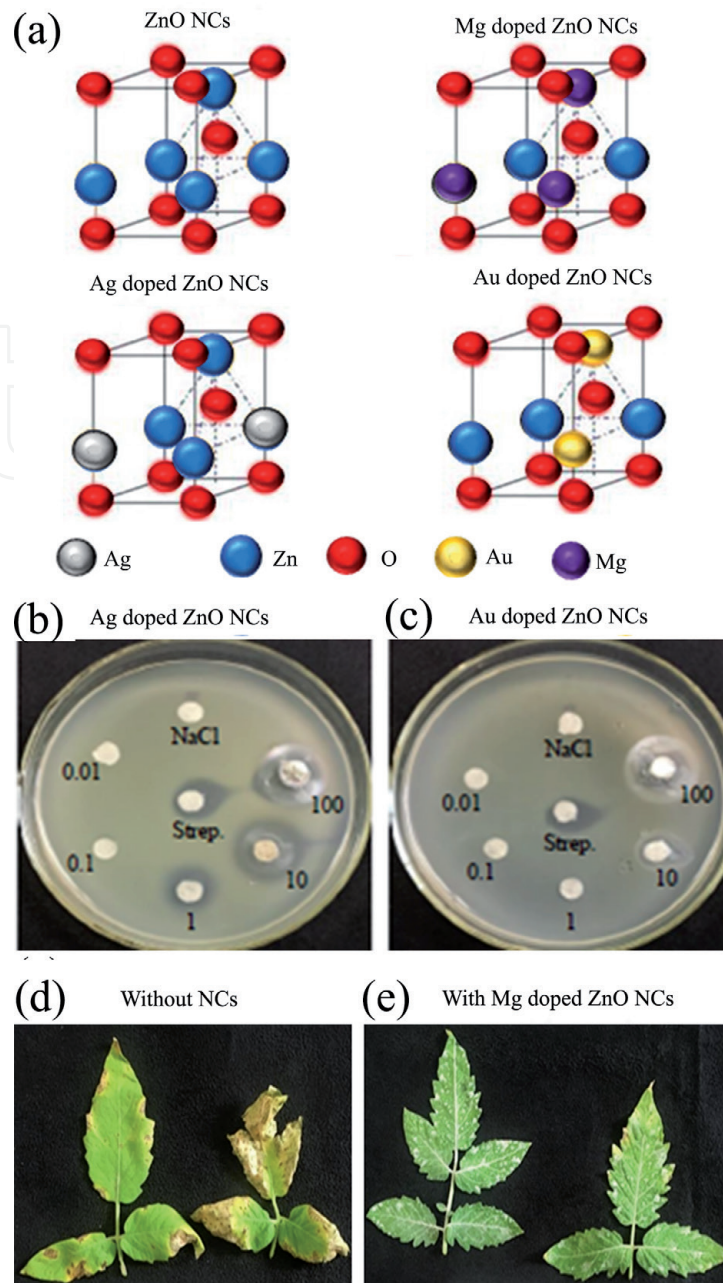


Figure 1. (a) Wurtzite structure of ZnO, Ag-doped ZnO, Au doped ZnO, and Mg-doped ZnO NCs. Growth inhibition zone for *Xanthomonas campestris* pv. *campestris* treated with (b) Ag-doped ZnO NCs and (c) Au doped ZnO NCs, at 100; 10; 1; 0.1; and 0.01 mg/mL. Strep. = streptomycin. Symptoms of bacterial spot-on tomato leaves, (d) caused by *Xanthomonas gardneri*, (e) with Mg-doped ZnO NCs showing disease control.

at Ag-doped $\text{Na}_2\text{Ti}_3\text{O}_7$ NCs exhibit a lethality rate 12.8% lower when compared to animals that developed on Na_2TiO_7 NCs, suggesting that Ag doping was able to increase the $\text{Na}_2\text{Ti}_3\text{O}_7$ NCs biocompatibility *in vivo* by decreasing its toxicity (Figure 2b).

As observed in Figure 3a, there was no delay in the time the larvae took to reach the pupal stage when exposed to $\text{Na}_2\text{Ti}_3\text{O}_7$ and Ag-doped $\text{Na}_2\text{Ti}_3\text{O}_7$ when compared to control. We have also performed an adult lifespan assay to evaluate the effects of NCs exposure during larval development and pupal metamorphosis over the adult survival. Therefore, after pupal metamorphosis, the animals that emerged as adults were immediately separated and kept in vials with standard control medium. These animals were transferred to a new vial with fresh standard medium every five days. The number of deaths for each experimental group was recorded daily until all individuals were dead. The lifetime of individuals that have developed in media

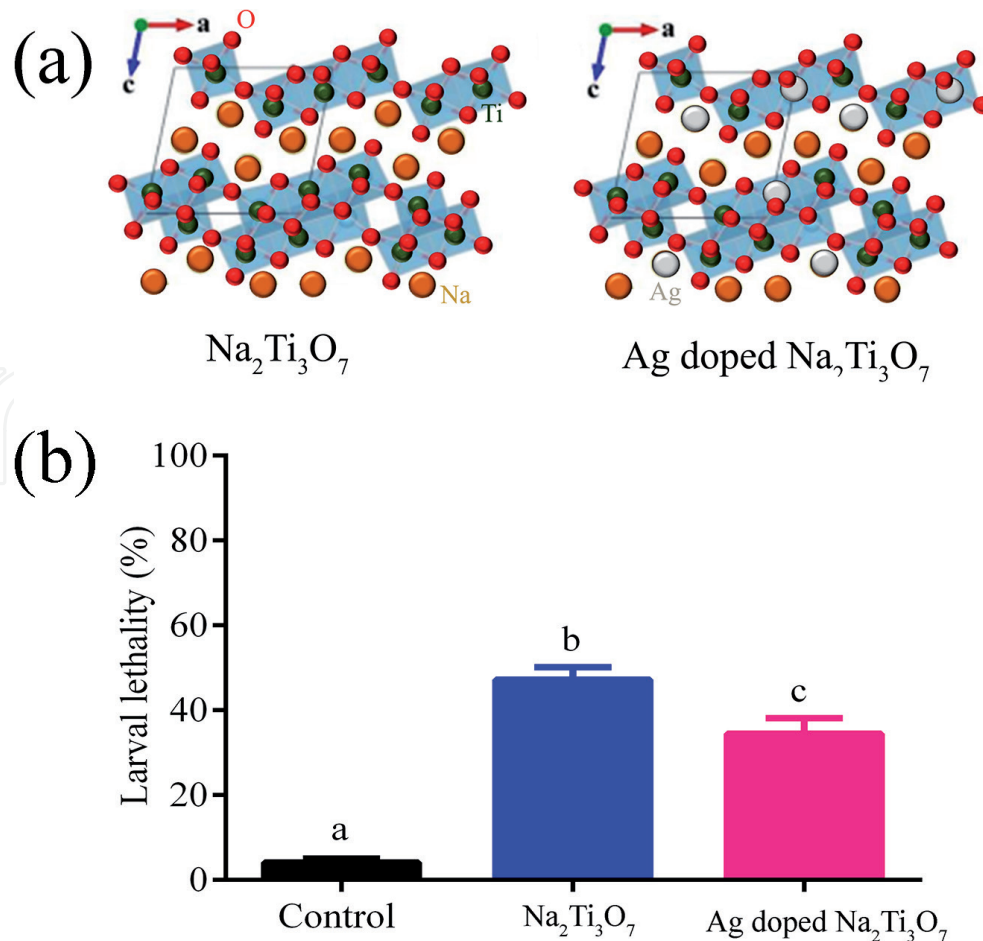


Figure 2. (a) Crystalline structure of pure and silver (Ag) doped sodium titanate ($\text{Na}_2\text{Ti}_3\text{O}_7$). (b) Larval lethality following NCs exposure. As observed $\text{Na}_2\text{Ti}_3\text{O}_7$ exposure caused a significant lethality rate during larval development, which was partially rescued by the Ag-doped $\text{Na}_2\text{Ti}_3\text{O}_7$.

containing $\text{Na}_2\text{Ti}_3\text{O}_7$ and Ag-doped $\text{Na}_2\text{Ti}_3\text{O}_7$ was compared to control animals that developed in a standard culture medium.

As shown in **Figure 3b** animals that developed in standard *Drosophila* medium containing $\text{Na}_2\text{Ti}_3\text{O}_7$ showed 20 days decrease in lifespan when compared to control. Surprisingly, the emerged adult flies that developed in medium containing Ag-doped $\text{Na}_2\text{Ti}_3\text{O}_7$ showed a longer longevity even when compared to animals that developed in standard culture medium or medium containing $\text{Na}_2\text{Ti}_3\text{O}_7$ NCs. Therefore, our data suggests that Ag-doped $\text{Na}_2\text{Ti}_3\text{O}_7$ was able to increase the $\text{Na}_2\text{Ti}_3\text{O}_7$ NCs biocompatibility *in vivo* by decreasing its toxicity.

The toxicity of NCs, such as zinc oxide, titanium dioxide, magnetite, hydroxyapatite, and sodium titanate, is induced through the generation of reactive species and consequent oxidative stress [33–35]. The redox imbalance caused by NCs is capable of generating mitochondrial dysfunctions, inducing inflammatory responses, causing cytotoxicity and genotoxicity, in addition to altering the functioning of the sodium and potassium channels and consequent cell death [33]. Oxidative stress not only causes cell damage and protein oxidation but is also possibly responsible for altering the biosynthesis of hormones, such as ecdysone in insects. Ecdysone is a crucial hormone in the control of metamorphosis and ecdysis events in insects [36, 37]. Our data showed a high larval lethality, especially in animals exposed to $\text{Na}_2\text{Ti}_3\text{O}_7$, possibly generated by oxidative stress, which can also impair ecdysone biosynthesis, causing developmental problems. One of the forgotten properties of NCs is their antioxidant capacity, such as Ag and cerium oxide

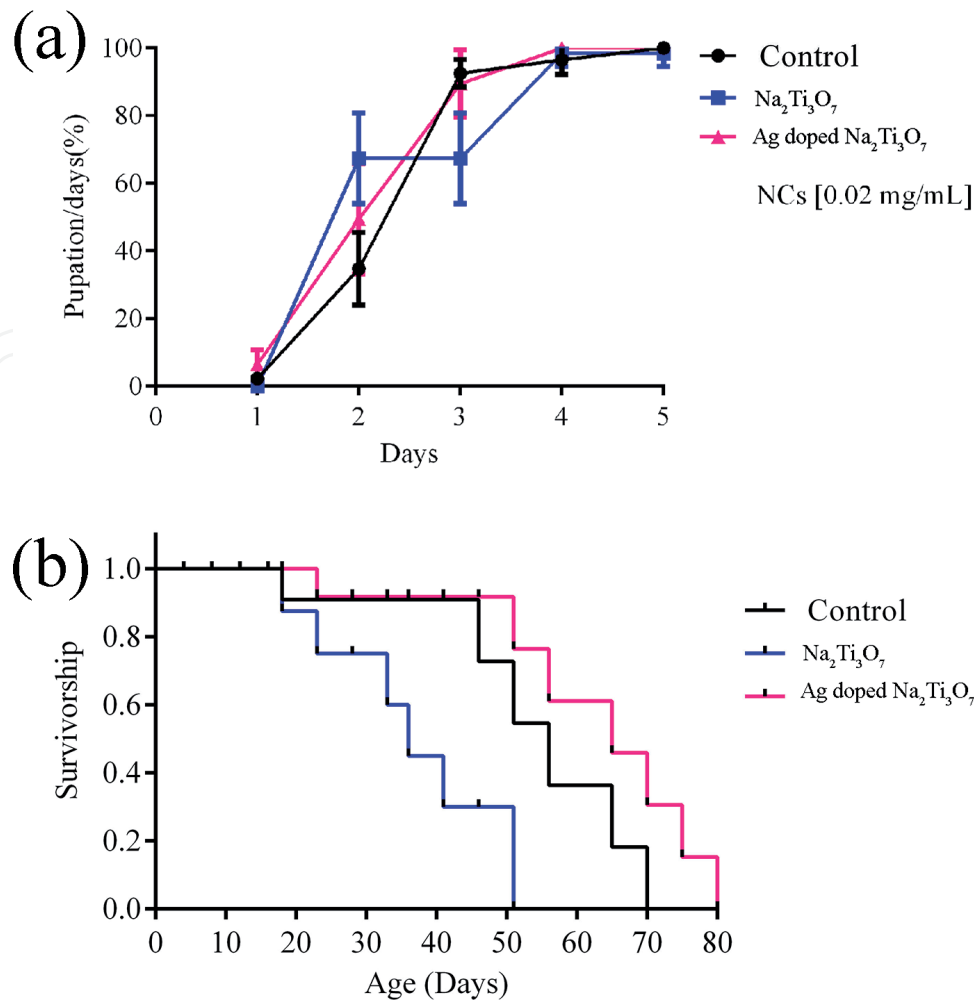


Figure 3.

(a) Daily pupation analysis of pure and Ag-doped $\text{Na}_2\text{Ti}_3\text{O}_7$ exposed animals. It is possible to observe that the exposure to pure and Ag-doped $\text{Na}_2\text{Ti}_3\text{O}_7$ Ag caused no delay in the transition from larva to pupa. (b) Lifespan analysis of pure and Ag-doped $\text{Na}_2\text{Ti}_3\text{O}_7$ exposed animals. It is shown that $\text{Na}_2\text{Ti}_3\text{O}_7$ exposure during development decreased adult longevity in about 20 days in comparison to control animals. However, the Ag-doped $\text{Na}_2\text{Ti}_3\text{O}_7$ not only rescued the animals survival but surprisingly increased it in 10 days in comparison to control animals.

nanoparticles (CONPs), and some NP of oxide that can even mimic an antioxidant molecule [38].

Therefore, we believe that the reduction in larval lethality observed for Ag-doped $\text{Na}_2\text{Ti}_3\text{O}_7$ NCs compared to $\text{Na}_2\text{Ti}_3\text{O}_7$ NCs can be explained by a lesser effect on the generation of reactive species, suggesting that the transition metal silver was sufficient to increase the biocompatibility of $\text{Na}_2\text{Ti}_3\text{O}_7$ NCs *in vivo*. However, additional studies are crucial to better understand the mechanisms by which development is influenced by nanocrystals.

2.3 Doped nanocrystals embedded in glass systems

This section will show the results of $\text{Zn}_{1-x}\text{Cr}_x\text{Te}$ NCs, $\text{Zn}_{1-x}\text{Cu}_x\text{Te}$ NCs, and $\text{Bi}_{2-x}\text{Cr}_x\text{Te}_3$ NCs embedded in glass systems aiming at spintronics applications.

2.3.1 Cr- and Cu-doped ZnTe nanocrystals embedded in glass matrix

Figure 4 presents TEM images (a) and X-ray diffraction (XRD) (b) of samples containing $\text{Zn}_{1-x}\text{Cr}_x\text{Te}$ NCs, with Cr-concentrations ranging from $x = 0.00$ to

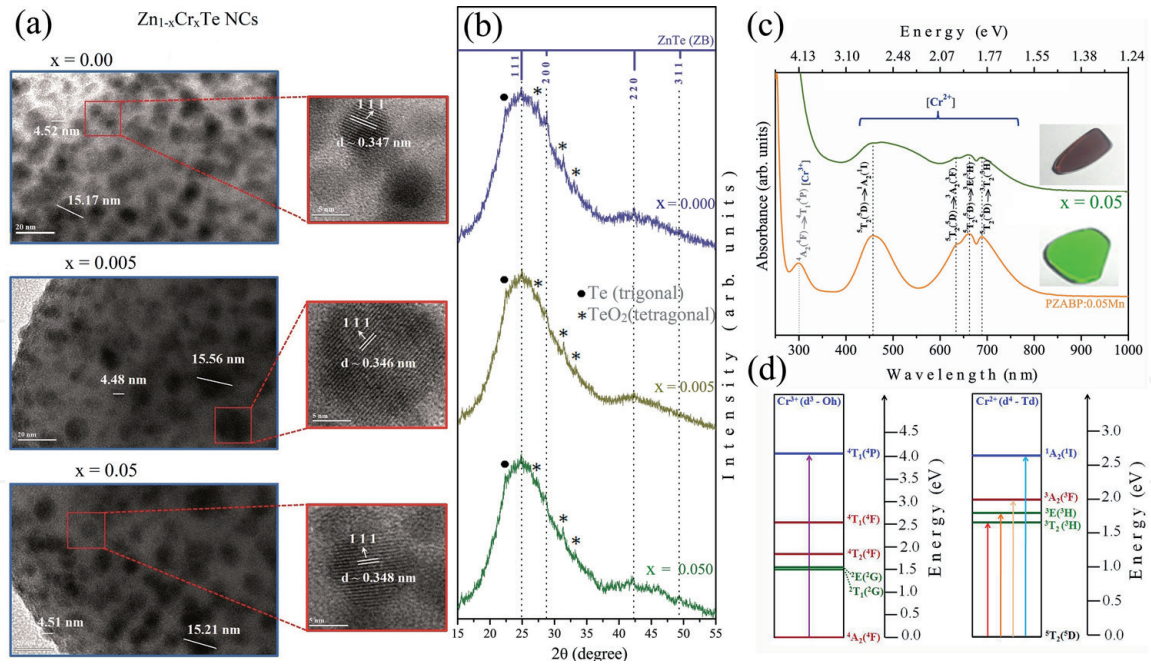


Figure 4.

TEM images (a) and XRD diffractograms (b) of samples containing Zn_{1-x}Cr_xTe NCs, with Cr-concentrations ranging from $x = 0.00$ to $x = 0.05$; (c) OA spectra of glass samples containing Zn_{1-x}Cr_xTe NCs, with concentration $x = 0.05$ and PZABP:0.05Cr; (d) energy diagram of Cr³⁺ and Cr²⁺ ions coordinated octahedral (oh) and tetrahedral (td).

$x = 0.05$. Already the **Figure 4(c)** shows OA spectra of glass samples containing Zn_{1-x}Cr_xTe NCs, with concentration $x = 0.05$ and PZABP glassy matrix doped with 0.05 Cr (PZABP:0.05Cr). In **Figure 4(d)**, energy diagram (below) of Cr³⁺ and Cr²⁺ ions coordinated octahedral (Oh) and tetrahedral (Td) of the transitions observed [22].

The formation of Zn_{1-x}Cr_xTe NCs was confirmed by Transmission Electron Microscopy (TEM) images. These images show two distinct groups of spherical NCs attributed to quantum dots (QDs) and bulk NCs, as we reported in our previous work [21]. The average diameters of these NCs are approximately $D \sim 4.50$ nm for QDs and $D \sim 15.31$ for bulk NCs. TEM images also show that the distance between their crystallographic planes of these does not vary with the Cr concentration. This suggests invariance in lattice parameter with the incorporation of Cr²⁺ ions. This result is expected, and is in accordance with what was observed from the XRD diffractograms, because the ionic radii of Zn²⁺ (0.68 nm) and Cr²⁺ (0.73 nm) are very similar. Thus, XRD show that the position of the peaks, corresponding to (1 1 1), (2 0 0) (2 2 0) and (3 1 1), is the same for all samples. Optical absorption spectra confirm the substitutional incorporation of Cr²⁺ ions in the ZnTe semiconductor lattice, due the ${}^5T_2({}^5D) \rightarrow {}^1A_2({}^1I)$, ${}^5T_2({}^5D) \rightarrow {}^3A_2({}^3F)$, ${}^5T_2({}^5D) \rightarrow {}^3E({}^3H)$ and ${}^5T_2({}^5D) \rightarrow {}^3T_2({}^3H)$ spin forbidden absorption bands of Cr²⁺ ions [39], indicated in the energy diagram.

Figure 5 shows OA spectra and photographs (a) of the PZABP template and of Zn_{1-x}Cu_xTe NC samples embedded in this template at different Cu-doping contents: x varying from 0.000 to 0.100. **Figure 5(b)** shows TEM images for sample with $x = 0.05$ (b) and EPR spectra for sample with $x = 0.10$ **Figure 5(c)** [21]. A redshift in the OA bands assigned to the QDs as Cu concentration increases, shifting from 3.10 eV (400 nm) to 2.95 eV (420 nm), when x ranges from 0.00 to 0.10. This decrease in the band gap energy with increase of transition metal (Cu) doped II-IV compound semiconductors can be best understand in terms of $sp-d$ spin exchange interaction between band electrons and the localized d electrons of the transition metal ions substituting the cations [40]. TEM images confirm the formation of

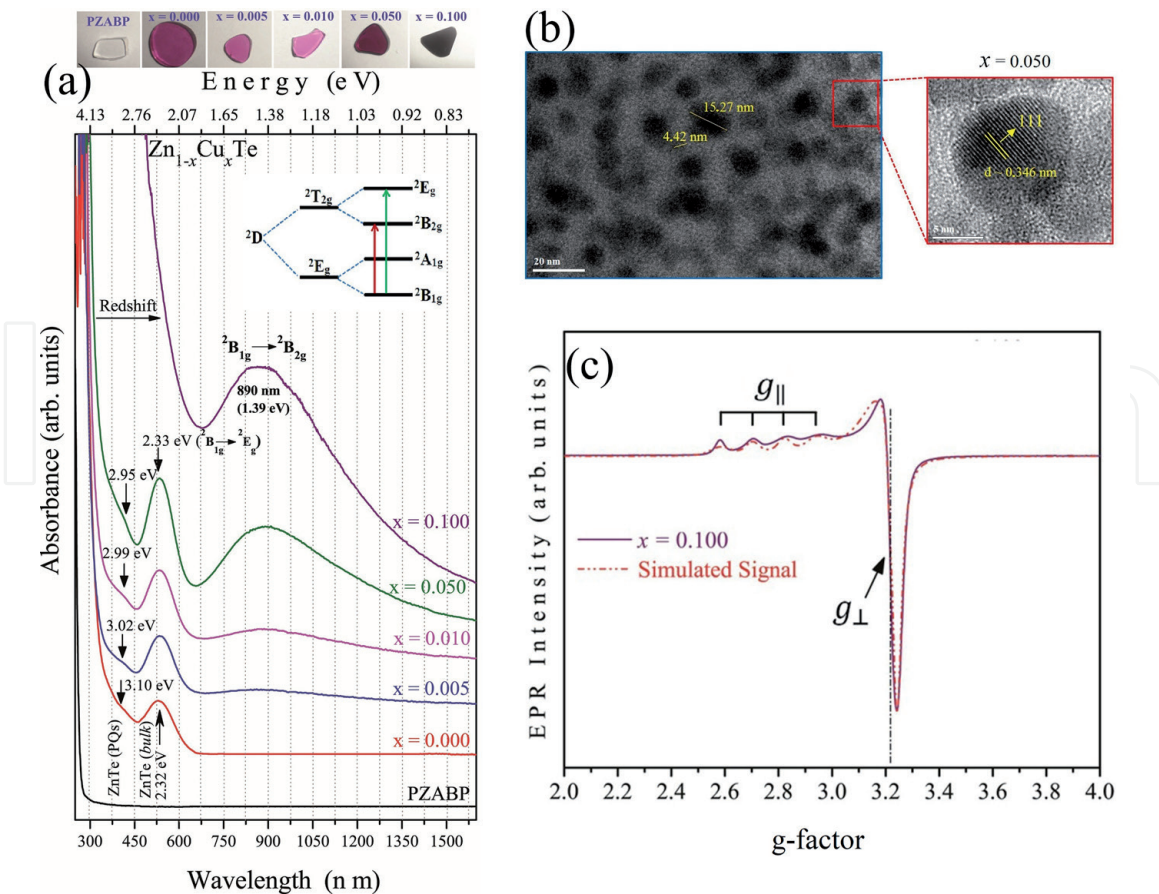


Figure 5. OA spectra and photographs (a) of the PZABP template and of Zn_{1-x}Cu_xTe NC samples embedded in this template at different Cu-doping contents: x varying from 0.00 to 0.100. TEM images for sample with x = 0.05 (b) and EPR spectra for sample with x = 0.10 (c).

Zn_{1-x}Cu_xTe NCs, with interplanar distance around d ~ 0.346 nm. Electron paramagnetic resonance spectra (EPR) confirm the substitutional incorporation, due to hyperfine transitions characteristic Cu²⁺ ions with d⁹ configuration.

2.3.2 Cr-doped Bi₂Te₃ nanocrystals embedded in glass systems

The UV-VIS optical absorption (OA) spectra shown in **Figure 6(a)** for the host glass matrix SNAB- 45SiO₂-30Na₂CO₃-5Al₂O₃-20B₂O₃ (mol%) of the Bi_{2-x}Cr_xTe₃ NCs with xCr molar fraction (x = 0.00; 0.01; 0.05) provides strong evidence of the formation and incorporation of Cr³⁺ ions in orthorhombic sites of Bi₂Te₃ NCs. The SNAB matrix with a band gap of approximately 4 eV [26], is an ideal template for observing d-d and excitonic transitions in Bi_{2-x}Cr_xTe₃ NCs as shown by the spectrum's bottom line (black) with no band in the visible region.

Bi₂Te₃ is a V - VI semiconductor that presents a narrow band gap of 0.13 eV in bulk form at room temperature [41]. The tail of the band attributed to the absorption of the charge carriers (electron-hole pair) shows the result of the nucleation and formation of the Bi₂Te₃ NCs with a confinement energy around 3.10 eV. The slight blueshift observed for the Bi_{2-x}Cr_xTe₃ NCs (x = 0.01; 0.05) is due to the strong sp-d exchange interactions between Bi₂Te₃ (sp) excitons and the electrons of the unoccupied 3d³ orbitals of the Cr³⁺ ion. This orbital coupling modifies the optical properties of the intrinsic semiconductor, proportional to the increase in Cr content. Finally, the sharpness of the bands of increasing intensity observed in the visible spectral region is due to the 3d-3d electronic transitions of the Cr ions [26, 42].

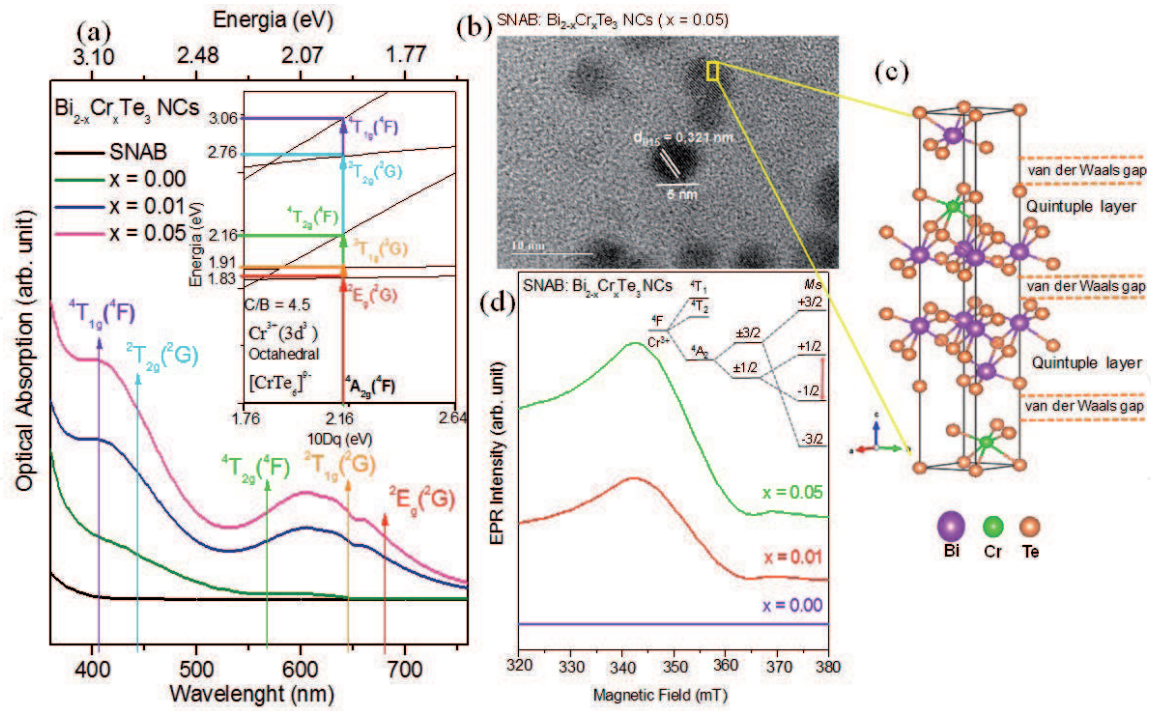


Figure 6.

(a) Optical absorption spectra at room temperature of $\text{Bi}_{2-x}\text{Cr}_x\text{Te}_3$ NCs ($x = 0.00; 0.01; 0.05$) embedded in SNAB glass matrix. For comparison purposes, the absorption spectrum of the SNAB glass matrix represents on the black bottom line. The inset shows the Tanabe-Sugano diagram d^3 of octahedral symmetry ($C/B = 4.5$) for the $[\text{CrTe}_6]^{9-}$ complex and the respective spin allowed and forbidden transitions indicated on the energy $10 Dq = 2.16$ eV. (b) TEM image of $\text{Bi}_{2-x}\text{Cr}_x\text{Te}_3$ NCs ($x = 0.05$) embedded in SNAB glass. (c) Details of the quintuple layer and the van der Waals gap in the Bi_2Te_3 hexagonal unit cell with the substitutional doping of Bi^{3+} ions by Cr^{3+} in distorted octahedral sites. (d) EPR spectra in the X band, at 300 K for NCs of $\text{Bi}_{2-x}\text{Cr}_x\text{Te}_3$ NCs ($x = 0.00; 0.01; 0.05$) embedded in the SNAB glass matrix. The inset shows the split diagram of the energy states of the system.

The energy states identified in the OA spectrum of figure x (a) belong to the spin allowed and forbidden d-d transitions: $^4A_2(^4F) \rightarrow ^2E_g(^2G)$ (1.83 eV), $^4A_2(^4F) \rightarrow ^2T_1(^2G)$ (1.91 eV), $^4A_2(^4F) \rightarrow ^4T_2(^4F)$ (2.16 eV), $^4A_2(^4F) \rightarrow ^2T_2(^2G)$ (2.76 eV) and $^4A_2(^4F) \rightarrow ^4T_1(^4F)$ (3.06 eV). These transitions are in accordance with a Tanabe-Sugano diagram d^3 of octahedral symmetry for $C/B = 4.5$ (see inset in **Figure 6a**) [43]. The results are typical of inter-electronic repulsion parameters (Racah) $B = 0.088$ eV in a crystal field strength $10 Dq (\Delta) = 2.16$ eV of Cr^{3+} ions in coordinated octahedral sites of Te ($[\text{CrTe}_6]^{9-}$) ligands [42, 44].

The exciton Bohr radius of approximately 50 nm for Bi_2Te_3 bulk [45] makes the semiconductor subject to strong quantum confinements. **Figure 6(b)** shows the TEM image of the SNAB glass matrix host of the $\text{Bi}_{2-x}\text{Cr}_x\text{Te}_3$ NCs ($x = 0.05$). The nanocrystal's 5 nm size confirms the formation of $\text{Bi}_{2-x}\text{Cr}_x\text{Te}_3$ quantum dots due to the strong quantum confinement of the semiconductor structure.

The quantum size of the $\text{Bi}_{2-x}\text{Cr}_x\text{Te}_3$ NCs does not change with the increase of Cr incorporation in the samples. In this way, the structure preserves due to the non-saturation of the molar fraction of Cr doping in the $\text{Bi}_{2-x}\text{Cr}_x\text{Te}_3$ NCs. The interplanar distance $d_{015} = 0.321$ nm is evidence of Tellurobismuthite's hexagonal crystalline structure [27, 41]. **Figure 6(c)** shows the hexagonal unit cell $R\bar{3}m - D_{3d}^5$ [41] of the Cr-doped Bi_2Te_3 NCs with the atomic arrangement of monoatomic planes Te - Cr - Te - Bi - Te and Te - Bi - Te - Bi - Te in terms of quintuple layers linked by weak van der Waals interactions [41]. The substitutional doping of Cr^{3+} ions with a smaller ionic radius (0.53 Å) in relation to Bi^{3+} (1.03 Å) distorts the environment of octahedral symmetry [42].

Figure 6(d) shows the EPR measurements in the X band, at 300 K for the $\text{Bi}_{2-x}\text{Cr}_x\text{Te}_3$ NCs ($x = 0.00; 0.01; 0.05$) samples embedded in the SNAB glass matrix. The EPR spectrum for Bi_2Te_3 not doped does not show any signal due to the absence of doping ions. However, the central signal characteristic of a $M_s = \pm 1/2$ transition typical of a fine structure line results from the interaction between the electronic ($S = 3/2$) and nuclear ($I = 0$) spins of Cr^{3+} ions in an octahedral crystal field. The inset in **Figure 6(d)** shows the split diagram of the energy states involved in the system. The increasing molar fraction of Cr ions in the $\text{Bi}_{2-x}\text{Cr}_x\text{Te}_3$ results in greater dipole–dipole interaction and, consequently, an increase in the observed RPE signal's intensity [26].

Therefore, the long-range magnetic properties generated by the domain of the Cr ion doping spins, in addition to the insulating topological states of the Bi_2Te_3 semiconductor NCs, have aroused great interest in the scientific community for the development of spintronic nanodevices [24, 25, 27, 28].

3. Conclusion

Therefore, this chapter showed the development and applications of several doped semiconductor nanocrystals, as nanopowders or embedded in glass systems. Doped Nanocrystals show good potential to control plant diseases as controlling bacterial diseases on field crops is complex. We also demonstrate that depending on the ion incorporated in the nanocrystal structure, the biocompatibility could be improved. Additionally, we show magnetic properties generated by the domain of the Cu or Cr ions doping spins, in addition to semiconductor nanocrystals embedded in glass systems, for the development of spintronic nanodevices.

Acknowledgements

This work was supported by grants of CNPq, CAPES, and FAPEMIG.

Conflict of interest

The authors declare no conflict of interest.

IntechOpen

Author details

Anielle C.A. Silva^{1,2*}, Eliete A. Alvin^{1,2}, Francisco R.A. dos Santos^{1,3},
Samanta L.M. de Matos^{1,3}, Jerusa M. de Oliveira³, Alessandra S. Silva⁴,
Éder V. Guimarães⁴, Mirella S. Vieira^{1,5}, Eurípedes A. da Silva Filho⁶,
Ricardo S. Silva⁴, Lucas Anhezini³, Nilvanira D. Tebaldi⁷ and Noelio O. Dantas^{1*}

1 Laboratory of New Nanostructured and Functional Materials, Physics Institute, Federal University of Alagoas, Maceió, Alagoas, Brazil

2 Programa de Pós-Graduação da Rede Nordeste de Biotecnologia (RENORBIO), Federal University of Alagoas, Maceió, Alagoas, Brazil

3 Laboratory for in vivo Toxicity, Institute of Biological Sciences and Health, Federal University of Alagoas, Maceió, Alagoas, Brazil

4 Instituto de Ciências Exatas, Naturais e Educação (ICENE), Departamento de Física, Federal University of Triângulo Mineiro, Minas Gerais, Brazil

5 Faculty of Electrical Engineering, Federal University of Uberlândia, Uberlândia, Brazil

6 Laboratory of Genetic and Applied Microbiology, Institute of Biological Sciences and Health, Federal University of Alagoas, Maceió, Alagoas, Brazil

7 Laboratory of Plant Bacteriology, Institute of Agricultural Sciences, Federal University of Uberlândia, Uberlândia, Brazil

*Address all correspondence to: acalmeida@fis.ufal.br and noelio@fis.ufal.br

IntechOpen

© 2021 The Author(s). Licensee IntechOpen. This chapter is distributed under the terms of the Creative Commons Attribution License (<http://creativecommons.org/licenses/by/3.0>), which permits unrestricted use, distribution, and reproduction in any medium, provided the original work is properly cited. 

References

- [1] Agrios, G.N. *Plant pathology*; 5th ed.; 2005;
- [2] Silva, A.; Zóia, M.A.P.; Correia, L.I.V.; Azevedo, F.V.P.V.; Paula, A.T. de; Maia, L.P.; Carvalho, L.S. de; Carvalho, L.N.; Costa, M.P.C.; Giaretta, L.C.; et al. Biocompatibility of Doped Semiconductors Nanocrystals and Nanocomposites. In *Cytotoxicity*; InTech, 2018.
- [3] Batista, E.A.; Silva, A.C.A.; de Lima, T.K.; Guimarães, E.V.; da Silva, R.S.; Dantas, N.O. Effect of the location of Mn²⁺ ions in the optical and magnetic properties of ZnO nanocrystals. *J. Alloys Compd.* **2021**, *850*, 156611, doi:10.1016/j.jallcom.2020.156611.
- [4] Souza, G.L. de; Moura, C.C.G.; Silva, A.C.A.; Marinho, J.Z.; Silva, T.R.; Dantas, N.O.; Bonvicini, J.F.S.; Turrioni, A.P. Effects of zinc oxide and calcium-doped zinc oxide nanocrystals on cytotoxicity and reactive oxygen species production in different cell culture models. *Restor. Dent. Endod.* **2020**, *45*, 54, doi:10.5395/rde.2020.45.e54.
- [5] Dantas, N.O.; Damigo, L.; Qu, F.; Cunha, J.F.R.; Silva, R.S.; Miranda, K.L.; Vilela, E.C.; Sartoratto, P.P.C.; Morais, P.C. Raman investigation of ZnO and Zn_{1-x}Mn_xO nanocrystals synthesized by precipitation method. *J. Non. Cryst. Solids* **2008**, *354*, 4827-4829, doi:10.1016/j.jnoncrsol.2008.04.051.
- [6] Naranjo, E.; Merfa, M. V.; Santra, S.; Ozcan, A.; Johnson, E.; Cobine, P.A.; De La Fuente, L. Zinkicide is a ZnO-based nanoformulation with bactericidal activity against *liberibacter crescens* in batch cultures and in microfluidic chambers simulating plant vascular systems. *Appl. Environ. Microbiol.* **2020**, *86*, 1-18, doi:10.1128/AEM.00788-20.
- [7] Maxwell, T.J.; Rajasekaran, P.; Young, M.; Schaff, M.; Heetai, R.; Santra, S. Non-phytotoxic zinc based nanoparticle adjuvant for improving rainfastness and sustained release of streptomycin. *Environ. Nanotechnology, Monit. Manag.* **2020**, *14*, 100355, doi:10.1016/j.enmm.2020.100355.
- [8] Liao, Y.-Y.; Strayer-Scherer, A.L.; White, J.; Mukherjee, A.; De La Torre-Roche, R.; Ritchie, L.; Colee, J.; Vallad, G.E.; Freeman, J.H.; Jones, J.B.; et al. Nano-Magnesium Oxide: A Novel Bactericide Against Copper-Tolerant *Xanthomonas perforans* Causing Tomato Bacterial Spot. *Phytopathology*® **2019**, *109*, 52-62, doi:10.1094/PHYTO-05-18-0152-R.
- [9] Zancan, N. Terapia fotodinâmica e nanopartículas no controle de *Xanthomonas campestris* pv. *campestris* in vitro e em sementes de canola naturalmente contaminadas, Universidade Federal de Uberlândia, 2018.
- [10] Mota, R.P. da Agressividade, caracterização molecular de isolados de *Pantoea ananatis* e nanopartículas no controle da bactéria na cultura do milho, Universidade Federal de Uberlândia: Uberlândia, 2019.
- [11] Mamede, M.C. Detecção de *Pantoea ananatis* em sementes de milho e nanopartículas no controle da bactéria in vitro, Universidade Federal de Uberlândia: Uberlândia, 2018.
- [12] Ballottin, D.; Fulaz, S.; Cabrini, F.; Tsukamoto, J.; Durán, N.; Alves, O.L.; Tasic, L. Antimicrobial textiles: Biogenic silver nanoparticles against *Candida* and *Xanthomonas*. *Mater. Sci. Eng. C* **2017**, *75*, 582-589, doi:10.1016/j.msec.2017.02.110.
- [13] Liang, Y.; Yang, D.; Cui, J. A graphene oxide/silver nanoparticle composite as a novel agricultural antibacterial agent against

- Xanthomonas oryzae pv. oryzae for crop disease management. *New J. Chem.* **2017**, *41*, 13692-13699, doi:10.1039/c7nj02942j.
- [14] Graham, J.H.; Johnson, E.G.; Myers, M.E.; Young, M.; Rajasekaran, P.; Das, S.; Santra, S. Potential of Nano-Formulated Zinc Oxide for Control of Citrus Canker on Grapefruit Trees. *Plant Dis.* **2016**, *100*, 2442-2447, doi:10.1094/PDIS-05-16-0598-RE.
- [15] Ong, C.; Yung, L.Y.L.; Cai, Y.; Bay, B.H.; Baeg, G.H. Drosophila melanogaster as a model organism to study nanotoxicity. *Nanotoxicology* **2015**, *9*, 396-403, doi:10.3109/17435390.2014.940405.
- [16] Reiter, L.T.; Potocki, L.; Chien, S.; Gribskov, M.; Bier, E. A systematic analysis of human disease-associated gene sequences in Drosophila melanogaster. *Genome Res.* **2001**, *11*, 1114-1125, doi:10.1101/gr.169101.
- [17] Pandey, U.B.; Nichols, C.D. Human disease models in Drosophila melanogaster and the role of the fly in therapeutic drug discovery. *Pharmacol. Rev.* **2011**, *63*, 411-436, doi:10.1124/pr.110.003293.
- [18] Counio, G.; Gacoin, T.; Boilot, J.P. Synthesis and photoluminescence of Cd_{1-x}MnxS (x ≤ 5%) nanocrystals. *J. Phys. Chem. B* **1998**, *102*, 5257-5260, doi:10.1021/jp980511w.
- [19] Hu, T.; Zhang, M.; Wang, S.; Shi, Q.; Cui, G.; Sun, S. CdS:Co diluted magnetic semiconductor nanocrystals: Synthesis and ferromagnetism study. *CrystEngComm* **2011**, *13*, 5646-5649, doi:10.1039/c1ce05593c.
- [20] Ogale, S.B. Dilute Doping, Defects, and Ferromagnetism in Metal Oxide Systems. *Adv. Mater.* **2010**, *22*, 3125-3155, doi:10.1002/adma.200903891.
- [21] Silva, A.S.; Pelegrini, F.; Figueiredo, L.C.; de Souza, P.E.N.; Morais, P.C.; Dantas, N.O. Effects of Cu²⁺ ion incorporation into ZnTe nanocrystals dispersed within a glass matrix. *J. Alloys Compd.* **2018**, *749*, 681-686, doi:10.1016/j.jallcom.2018.03.290.
- [22] Silva, A.S.; Lourenço, S.A.; Da Silva, M.A.T.; Dantas, N.O. Optical properties of Cr-doped Zn_{1-x}MnxTe semimagnetic nanocrystals. *Appl. Phys. Lett.* **2018**, *112*, doi:10.1063/1.5016382.
- [23] Qi, X.; Ma, W.; Zhang, X.; Zhang, C. Raman characterization and transport properties of morphology-dependent two-dimensional Bi₂Te₃ nanofilms. *Appl. Surf. Sci.* **2018**, *457*, 41-48, doi:10.1016/j.apsusc.2018.06.142.
- [24] Irfan, S.; Luo, J.; Ping, F.; Zhuanghao, Z. Theoretical and experimental investigation of magnetic properties of iodine and cerium Co-doped Bi₂Te₃ nanoparticles. *J. Mater. Res. Technol.* **2020**, *9*, 13893-13901, doi:10.1016/j.jmrt.2020.09.086.
- [25] Silva, R.S.; Gualdi, A.J.; Zabetto, F.L.; Cano, N.F.; Silva, A.C.A.; Dantas, N.O. Weak ferromagnetism in Mn²⁺ doped Bi₂Te₃ nanocrystals grown in glass matrix. *J. Alloys Compd.* **2017**, *708*, 619-622, doi:10.1016/j.jallcom.2017.03.066.
- [26] Araujo, C.M.; Mikhail, H.D.; Guimarães, E. V.; Rastrello, L.R.; Cano, N.F.; Silva, A.C.A.; Dantas, N.O.; Silva, R.S. Optical, structural and magnetic characterization of Bi_{2-x}CrxTe₃ nanocrystals in oxide glass. *Mater. Chem. Phys.* **2020**, *241*, doi:10.1016/j.matchemphys.2019.122323.
- [27] Silva, R.S.; Mikhail, H.D.; Pavani, R.; Cano, N.F.; Silva, A.C.A.; Dantas, N.O. Synthesis of diluted magnetic semiconductor Bi_{2-x}MnxTe₃ nanocrystals in a host glass matrix. *J. Alloys Compd.* **2015**, *648*, 778-782, doi:10.1016/j.jallcom.2015.07.045.
- [28] Fert, A.; Van Dau, F.N. Spintronics, from giant magnetoresistance to

magnetic skyrmions and topological insulators. *Comptes Rendus Phys.* 2019, 20, 817-831.

[29] Silva, A.; Zóia, M.A.P.; Correia, L.I.V.; Azevedo, F.V.P.V.; Paula, A.T. de; Maia, L.P.; Carvalho, L.S. de; Carvalho, L.N.; Costa, M.P.C.; Giaretta, L.C.; et al. Biocompatibility of Doped Semiconductors Nanocrystals and Nanocomposites. In *Cytotoxicity*; InTech, 2018.

[30] Umek, P.; Gloter, A.; Navio, C.; Bittencourt, C. Synthesis and characterization of sodium titanate and TiO₂ nanostructures loaded with silver nanoparticles. In *Proceedings of the AIP Conference Proceedings*; American Institute of Physics AIP, 2011; Vol. 1415, pp. 24-27.

[31] Fraga, F. Controle de *Xanthomonas* spp. com nanocristais de ZnO puros e dopados no tomateiro, Universidade Federal de Uberlândia, 2020.

[32] Elmer, W.; White, J.C. The future of nanotechnology in plant pathology. *Annu. Rev. Phytopathol.* 2018, 56, 111-133.

[33] Manke, A.; Wang, L.; Rojanasakul, Y. Mechanisms of nanoparticle-induced oxidative stress and toxicity. *Biomed Res. Int.* 2013, 2013, doi:10.1155/2013/942916.

[34] Ajdary, M.; Moosavi, M.A.; Rahmati, M.; Falahati, M.; Mahboubi, M.; Mandegary, A.; Jangjoo, S.; Mohammadinejad, R.; Varma, R.S. Health concerns of various nanoparticles: A review of their in vitro and in vivo toxicity. *Nanomaterials* 2018, 8, 1-28, doi:10.3390/nano8090634.

[35] Singh, A.; Raj, A.; Shah, P.; Agrawal, N. Synthesis and Characterization of Nanoparticles Used in Consumer Products. In *Toxicology of Nanoparticles: Insights from Drosophila*; Springer Singapore, 2020; pp. 1-27.

[36] Uryu, O.; Ameku, T.; Niwa, R. Recent progress in understanding the role of ecdysteroids in adult insects: Germline development and circadian clock in the fruit fly *Drosophila melanogaster*. *Zool. Lett.* 2015, 1, 1-9, doi:10.1186/s40851-015-0031-2.

[37] Yamanaka, N.; Marqués, G.; O'Connor, M.B. Vesicle-Mediated Steroid Hormone Secretion in *Drosophila melanogaster*. *Cell* 2015, 163, 907-919, doi:10.1016/j.cell.2015.10.022.

[38] Kumar, H.; Bhardwaj, K.; Nepovimova, E.; Kuča, K.; Dhanjal, D.S.; Bhardwaj, S.; Bhatia, S.K.; Verma, R.; Kumar, D. Antioxidant functionalized nanoparticles: A combat against oxidative stress. *Nanomaterials* 2020, 10, 1-31, doi:10.3390/nano10071334.

[39] Nitsuk, Y.A. Energy states of a Cr²⁺ ion in ZnSe crystals. *Semiconductors* 2013, 47, 736-739, doi:10.1134/S1063782613060183.

[40] Rusu, G.I.; Diciu, M.; Pîrghie, C.; Popa, E.M. Structural characterization and optical properties of ZnSe thin films. *Appl. Surf. Sci.* 2007, 253, 9500-9505, doi:10.1016/j.apsusc.2007.06.009.

[41] Deng, J.; Zhao, Z.Y. Electronic structure and optical properties of bismuth chalcogenides Bi₂Q₃ (Q = O, S, Se, Te) by first-principles calculations. *Comput. Mater. Sci.* 2018, 142, 312-319, doi:10.1016/j.commatsci.2017.10.032.

[42] Guimarães, É. V.; Mikhail, H.D.; Silva, A.C.A.; Dantas, N.O.; Silva, R.S. Investigations of structural and optical properties of Bi_{2-x}Cr_xS₃ nanocrystals embedded in host glass. *Mater. Lett.* 2020, 265, doi:10.1016/j.matlet.2020.127430.

[43] Tanabe, Y.; Sugano, S. On the Absorption Spectra of Complex Ions. *J. Phys. Soc. Japan* 1954, 9, 753-766, doi:10.1143/JPSJ.9.753.

[44] Navas, A.S.; Reddy, B.J.; Nieto, F. Spectroscopic study of chromium, iron, OH, fluid and mineral inclusions in uvarovite and fuchsite. *Spectrochim. Acta - Part A Mol. Biomol. Spectrosc.* **2004**, *60*, 2261-2268, doi:10.1016/j.saa.2003.11.024.

[45] Bejenari, I.; Kantser, V.; Balandin, A.A. Thermoelectric properties of electrically gated bismuth telluride nanowires. *Phys. Rev. B - Condens. Matter Mater. Phys.* **2009**, *81*, 075316, doi:10.1103/PhysRevB.81.075316.

IntechOpen